

Article

Exploring the Venom Diversity of Australian Taipans: Comparative Characterization of *Oxyuranus microlepidotus* and *Oxyuranus scutellatus*

Guilherme Gonelli Paz^{1,2}, Patrick Jack Spencer³, Daniel Carvalho Pimenta⁴ and Emidio Beraldo-Neto^{2,*}

¹ Programa de Pós-Graduação em Ciências—Toxinologia do Instituto Butantan, São Paulo 05503-900, SP, Brazil; guilherme_gonelli@outlook.com

² Laboratory of Biochemistry, Instituto Butantan, São Paulo 05503-900, SP, Brazil

³ Instituto de Pesquisas Energéticas e Nucleares, São Paulo 05508-000, SP, Brazil; pspencer@ipen.br

⁴ Laboratório de Ecologia e Evolução, Instituto Butantan, São Paulo 05503-900, SP, Brazil; dcpimenta@butantan.gov.br

* Correspondence: emidio.beraldo@butantan.gov.br

Abstract

The genus *Oxyuranus*, which includes some of the most venomous snakes in the world, presents a complex venom composition with potent neurotoxic and procoagulant effects. This study provides a comparative proteomic analysis of the venom of *Oxyuranus microlepidotus* (Inland Taipan) and *Oxyuranus scutellatus* (Coastal Taipan), aiming to elucidate the molecular basis underlying their distinct toxicological profiles. Using high-resolution chromatographic fractionation and LC-MS/MS, we identified a core set of nine protein families shared between both species, including phospholipases A₂ (PLA₂), three-finger toxins (3FTx), natriuretic peptides (NTP), nerve growth factors (NGF), and prothrombin activators (PTA). *O. microlepidotus* venom exhibited greater diversity of 3FTxs and unique protein families, such as Waprin and 5'-nucleotidases, suggesting lineage-specific functional adaptations. Quantitative analysis revealed a greater relative abundance of PLA₂s in *O. scutellatus* (66%) compared to *O. microlepidotus* (47%), whereas 3FTxs were more prominent in *O. microlepidotus* (33% vs. 9%). These interspecific differences likely underlie the distinct clinical manifestations of envenomation and reflect evolutionary divergence in the venom composition. Our findings provide molecular insights into taipan venom complexity and highlight novel toxin candidates with potential biomedical applications in neurobiology, hemostasis, and anti-infective therapy.



Received: 27 August 2025

Revised: 24 September 2025

Accepted: 25 September 2025

Published: 1 October 2025

Citation: Paz, G.G.; Spencer, P.J.; Pimenta, D.C.; Beraldo-Neto, E. Exploring the Venom Diversity of Australian Taipans: Comparative Characterization of *Oxyuranus microlepidotus* and *Oxyuranus scutellatus*. *Toxins* **2025**, *17*, 488. <https://doi.org/10.3390/toxins17100488>

Copyright: © 2025 by the authors. Licensee MDPI, Basel, Switzerland. This article is an open access article distributed under the terms and conditions of the Creative Commons Attribution (CC BY) license (<https://creativecommons.org/licenses/by/4.0/>).

Keywords: taipan venom; proteomics; *Oxyuranus scutellatus*; *Oxyuranus microlepidotus*; Inland Taipan; Coastal Taipan

Key Contribution: Comprehensive comparative proteomic analysis of *Oxyuranus microlepidotus* and *Oxyuranus scutellatus* venoms reveals nine shared protein families and highlights striking quantitative and qualitative differences—such as elevated PLA₂ in *O. scutellatus* (66% vs. 47%) and enriched 3FTx in *O. microlepidotus* (33% vs. 9%)—suggesting an evolutionary basis for the higher lethality of the Inland Taipan. The unique presence of Waprin and 5'-nucleotidase in *O. microlepidotus* venom further supports its distinct molecular profile and unveils promising candidates for therapeutic exploration in neurobiology, antimicrobial strategies, and hemostasis.

1. Introduction

Australia is widely known for its biodiversity, especially regarding the presence of venomous and poisonous animals, including snakes [1–3]. Among the main snake families found on Australian territory, the *Elapidae* family stands out, whose members are known for their highly toxic venoms, with emphasis on the *Oxyuranus* genus, which includes the most venomous snakes in the world [3–7]. The main representatives of this genus include *O. scutellatus scutellatus* (Coastal Taipan), *O. microlepidotus* (Inland Taipan), *O. temporalis* (Central Ranges Taipan) and *O. scutellatus canni* (Papuan Taipan), the latter being found outside Australian territory [8–10].

Clinically, envenomation by snakes of the *Oxyuranus* genus is characterized by a set of neurotoxic and cytotoxic manifestations, including thrombocytopenia, rhabdomyolysis, acute kidney injury, and descending paralysis, which may progress to respiratory failure [7,11,12]. These clinical manifestations result from the action of various toxins present in the venom of these snakes, with taipoxin being one of the main neurotoxic components. Belonging to the phospholipase A₂ family, this toxin induces paralysis by causing neurotransmitter depletion at motor nerve terminals [13–17]. Additionally, taipoxin exerts myotoxic effects through the hydrolysis of muscle fiber membranes [17].

Alongside taipoxin, taipotoxin, another toxin present in taipan venom, contributes to neurotoxic effects by blocking voltage-gated calcium channels (CaV), interfering with neurotransmission [18–20]. Several other toxins have been characterized in the venom of these animals, including natriuretic toxins, associated with nephrotoxic effects; prothrombin activators, responsible for coagulopathic disorders; and multiples phospholipases A₂ [21–24]. Despite the similarity of compounds found in the venom of these taipan species, studies indicate that lethality varies between species [25,26]. Evidence suggests that *O. microlepidotus* has higher lethality compared to other taipan species and is considered the most venomous snake in the world. Nevertheless, its venom remains relatively underexplored, with few studies focused on its composition.

Several studies have investigated the venom composition of *Oxyuranus* species, employing chromatographic profiling, mass analyses, and assessment of molecular activity [8,27,28]. Nevertheless, only one study, conducted by Herrera et al. [22], has provided a comprehensive characterization of the venom of *O. scutellatus scutellatus*, in comparison with that of *O. scutellatus canni*, a subspecies found in Papua New Guinea. This study revealed a range of shared venom components between two species; however, significant quantitative differences were observed, which may account for the variation in toxicity reported between them.

Given the high specificity and potency of snake venom toxins, characterizing these molecules may also yield candidates for therapeutic development or molecular tools to study physiological processes, particularly in neurobiology and hemostasis.

Therefore, this study aims to characterize the venom of *O. microlepidotus* using proteomic approaches and compare it with the venom of *O. scutellatus*. We hypothesize that compositional differences between these species may underlie the distinct clinical outcomes of envenomation and reveal novel bioactive molecules with potential biomedical applications.

2. Results and Discussion

2.1. Venom Profile

Proteomic analyses revealed the presence of nine common protein families in the venoms of *O. microlepidotus* and *O. scutellatus*, including phospholipases A₂ (PLA₂), three-finger toxins (3FTxs), nerve growth factors (NGFs), prothrombin activators (PTAs), natriuretic peptides (NPs), cysteine-rich secretory proteins (CRISPs), BPTI/Kunitz protease inhibitors,

and carboxypeptidases (Figures 1 and 2). Among these, PLA₂ and 3FTxs stand out as the major effector molecules, being directly responsible for most of the neurotoxic and systemic effects of taipan venoms. For this reason, these two toxin families are given priority in the discussion, with emphasis on their biochemical diversity and comparative roles between the species. In addition, the proteome of *O. microlepidotus* revealed the presence of a Waprin family protein, absent in *O. scutellatus*. Waprins are structurally related to WAP (Whey Acidic Proteins) and are known for their roles in innate immunity and immunomodulation, representing a noteworthy finding that broadens the functional landscape of taipan venoms [29,30].

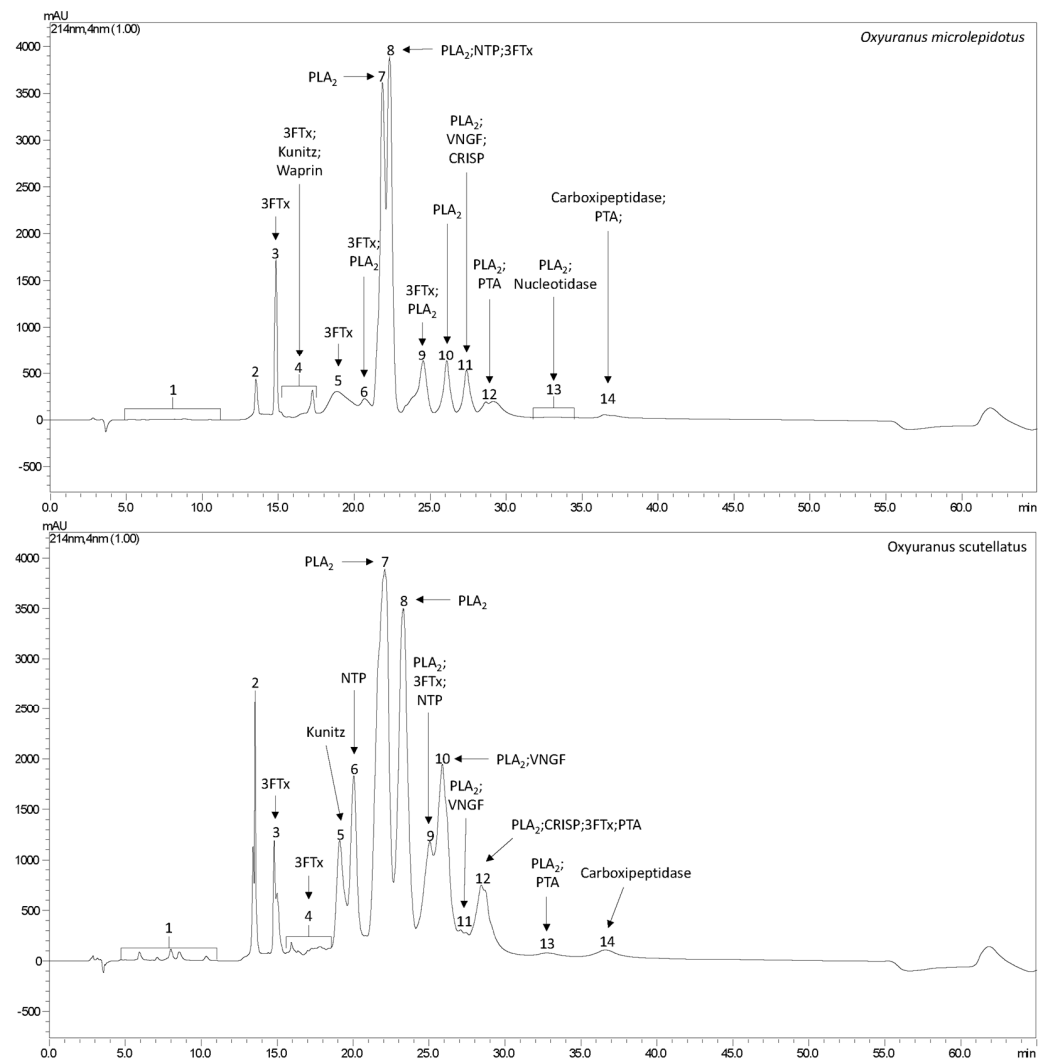


Figure 1. Chromatographic profile of *O. microlepidotus* and *O. scutellatus*, showing the compounds identified within the respective fractions.

The Waprin identified in the venom of *O. microlepidotus* designated Omwaprin-b (B5G6G7), is a protein that shares 94% sequence identity with a previously described protein from the same species, Omwaprin-a (P83952). This protein has demonstrated antimicrobial activity through membrane disruption, without exhibiting toxicity in mice or hemolytic activity, indicating both high specificity and potent antimicrobial efficacy [31]. Furthermore, two synthetic peptides derived from Omwaprin—OMW1 and OMW2—showed even greater antimicrobial potential, effectively inhibiting *Candida albicans* biofilm formation and inducing complete lysis of *Escherichia coli* and *Staphylococcus aureus*, further highlighting the strong bioactive potential of this toxin [32].

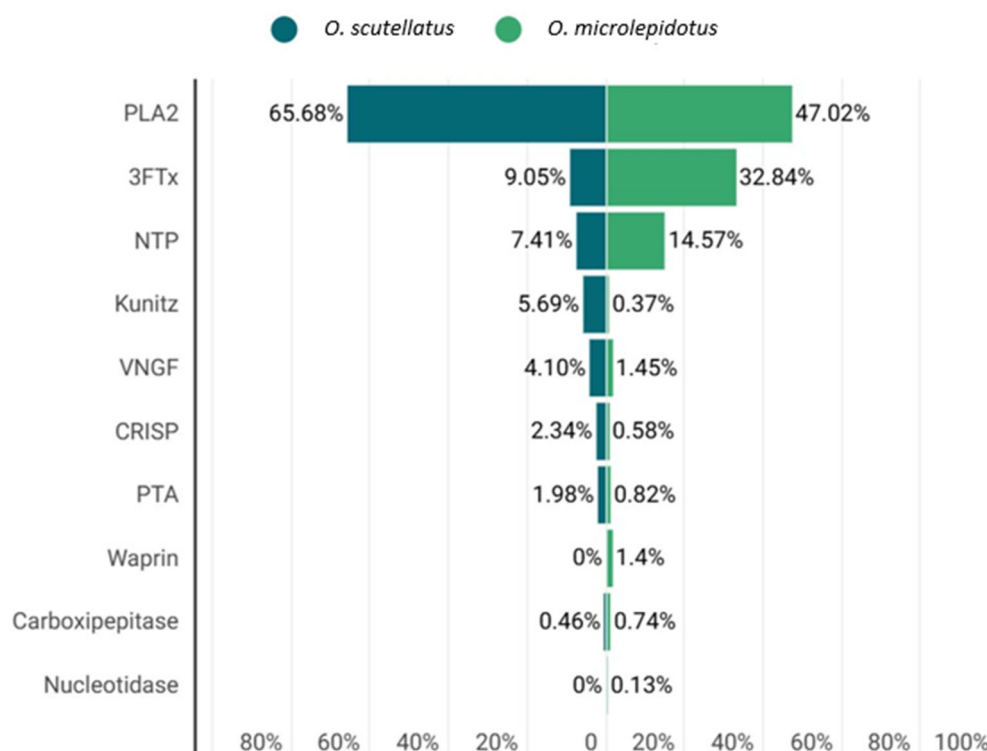


Figure 2. Comparative quantitative analysis of protein families identified in *O. scutellatus* and *O. microlepidotus*.

The structural analysis of Omwaprin-b (B5G6G7) identified a single binding pocket (Figure 3) with distinct physicochemical properties. The pocket displays a moderate drugability score (0.49) and a relatively small volume (103 \AA^3), suggesting a selective interaction site for small molecules or lipid head groups. Its strongly hydrophilic character, reflected by high polarity (11.0) and negative hydrophobicity (-2.2), indicates a preference for polar or charged targets, such as phospholipid head groups or peptidoglycan components in bacterial membranes. Moreover, the high solvent-accessible surface area (1262 \AA^2) combined with a balanced polar/apolar ratio (0.91) suggests broad accessibility, which may favor initial recognition and anchoring to bacterial membranes.

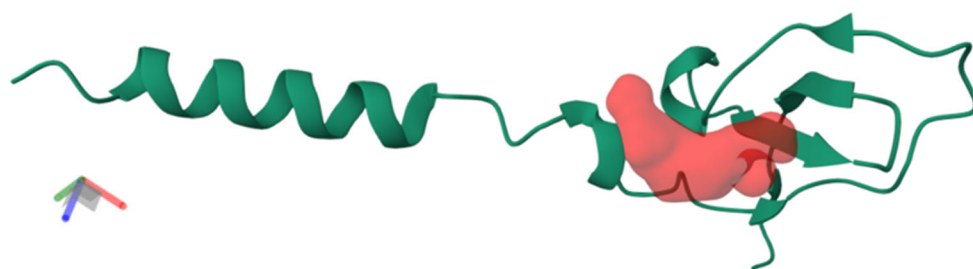


Figure 3. Three-dimensional structure of Omwaprin-b (B5G6G7) highlighting the identified Red Pocket. The protein backbone is represented as a ribbon diagram, while the Red Pocket is shown as a surface cavity centered at coordinates $[-8.2, 7.8, 1.9]$. Pocket features include a relatively small volume (103 \AA^3), high polarity, and moderate drugability score (0.49), consistent with selective recognition of polar membrane components and a potential role in antimicrobial activity.

These structural features are consistent with the proposed mechanism of action of cysteine-rich antimicrobial peptides, in which pocket-mediated recognition precedes membrane disruption. In the case of Omwaprin-b, the Red Pocket may function as a selective anchoring site that facilitates interaction with bacterial membrane components, ultimately

leading to destabilization of bilayer integrity and cell death. This aligns with established models of antimicrobial peptide function that emphasize selective binding to bacterial versus mammalian membranes. However, since these insights are derived from computational prediction, further experimental validation is necessary to confirm the specific molecular partners and to establish the functional contribution of this pocket to Omwaprin-b's antimicrobial activity.

In addition to the Waprin family, two proteins (A0A670YUG0; A0A2I4HXH5) belonging to the 5'-nucleotidase family were also identified in the venom of *O. microlepidotus*. The proteins share high sequence identity (96%). Although the role of these enzymes in the snake venoms is not fully understood, studies suggest that their primary function is the generation of purines, which may contribute to central nervous system depression. Additionally, they have been implicated in hemostatic modulation through the inhibition of platelet aggregation [33].

Table 1 (*O. microlepidotus*) and Table 2 (*O. scutellatus*) summarize the proteins identified in the proteomic analysis.

Table 1. Identified proteins in the venom of *O. microlepidotus* by proteomic analysis.

Fraction	UNIPROT Code	Theoretical Mass (kDa) ¹	−10lgP	Peptides	Unique Peptides	Protein Description	Type
3	A7X4S0	6.79	137.57	8	8	Short neurotoxin 3FTx-Oxy4 (<i>O. microlepidotus</i>)	3FTx
4	P0CB06 ^{F4}	6.79	64.89	3	1	Short neurotoxin 2 (<i>O. scutellatus</i>)	3FTx
	B7S4N9 ^{F5}	7	61.68	3	3	Kunitz-type protease inhibitor taicotoxin (<i>O. scutellatus</i>)	Kunitz
	B5G6G7	5.72	119.78	12	12	Omwaprin-b (<i>O. microlepidotus</i>)	Waprin
5	A7X4R0	7.91	137.90	8	1	Long neurotoxin 3FTx-Oxy2 (<i>O. microlepidotus</i>)	3FTx
6	Q45Z49	14.32	85.63	4	1	PLA-5 (<i>O. scutellatus</i>)	PLA ₂
	A8HDK8	7.98	191.13	16	1	Long neurotoxin 2 (<i>O. microlepidotus</i>)	3FTx
	A7X4Q3	7.95	188.04	16	1	Long neurotoxin 3FTx- Oxy1 (<i>O. microlepidotus</i>)	3FTx
7	Q45Z41	14.22	152.09	12	4	PLA-5 (<i>O. microlepidotus</i>)	PLA ₂
8	Q4VRI7 ^{F8}	14.35	99.72	5	1	Alpha taipoxin-2 (<i>O. scutellatus</i>)	PLA ₂
	A7X4S7	6.28	102.05	4	4	Toxin 3FTx- Oxy5 (<i>O. microlepidotus</i>)	3FTx
	Q3SAF8	4.11	123.71	6	6	Natriuretic peptide OmNP-d (fragment) (<i>O. microlepidotus</i>)	NP
9	P00614 ^{F9}	13.83	138.13	12	6	Basic phospholipase A2 taipoxin alpha chain (<i>O. scutellatus</i>)	PLA ₂
	A7X4T2 ^{F12}	6.87	129.48	6	6	Three-finger Toxin 3FTx-Oxy6 (<i>O. microlepidotus</i>)	3FTx
	A8HDK2 ^{F9}	6.34	66.99	3	3	Short neurotoxin 3 (<i>O. scutellatus</i>)	3FTx
10	Q45Z45 ^{F9}	15	173.78	18	6	PLA-1 (<i>O. microlepidotus</i>)	PLA ₂
	Q45Z51 ^{F10}	14.95	159.33	12	2	PLA-3 (<i>O. microlepidotus</i>)	PLA ₂
	P0CG57	13.31	115.25	5	1	Neutral phospholipase A2 homolog taipoxin beta chain 2 (<i>O. microlepidotus</i>)	PLA ₂

Table 1. Cont.

Fraction	UNIPROT Code	Theoretical Mass (kDa) ¹	−10lgP	Peptides	Unique Peptides	Protein Description	Type
11	Q45Z46 ^{F10}	13.33	184.44	22	10	Neutral phospholipase A2 paradoxin-like beta chain (<i>O. microlepidotus</i>)	PLA ₂
	P00615 ^{F11}	13.23	99.21	6	1	Neutral phospholipase A2 homolog taipoxin beta chain 1 (<i>O. scutellatus</i>)	PLA ₂
	Q3HXZ0 ^{F10}	13.39	116.17	5	5	Venom nerve growth factor 2 (<i>O. microlepidotus</i>)	NGF
	Q3SB07 ^{F12}	23.55	83.52	3	2	Cysteine-rich venom protein pseudochetoxin-like (<i>O. scutellatus</i>)	CRISP
12	P00616 ^{F12}	14.60	214.03	27	16	Acidic phospholipase A2 homolog taipoxin gamma chain (<i>O. scutellatus</i>)	PLA ₂
	Q9PUH0	13.44	53.51	2	1	Acidic phospholipase A2 S8-51 (<i>Austrelaps superbus</i>)	PLA ₂
	Q58L95	15.99	85.41	3	3	Venom prothrombin activator omicarin-C catalytic subunit (<i>O. microlepidotus</i>)	PTA
	P60043	13.21	63.09	3	1	Basic phospholipase A2 1 (Fragment) (<i>Naja. Sagittifera</i>)	PLA ₂
13	Q45Z50 ^{F13}	15.21	171.55	5	2	PLA-4 (<i>O. scutellatus</i>)	PLA ₂
	Q4VRI5 ^{F9}	14.10	123.21	4	1	Phospholipase A2 OS1 (<i>O. scutellatus</i>)	PLA ₂
	A0A670YUG0	48.31	74.98	3	1	5' nucleotidase ecto (<i>Pseudonaja textilis</i>)	Nucleotidase
	A0A2I4HXH5	57.81	70.13	3	1	Snake venom 5'-nucleotidase (<i>Naja atra</i>)	Nucleotidase
14	A0A670Y1M6 ^{F14}	53.81	134.99	12	6	Prolylcarboxypeptidase (<i>Pseudonaja textilis</i>)	Peptidase
	A0A8C6XE75	51.58	107.01	8	1	Prolylcarboxipeptidase (<i>Naja naja</i>)	Peptidase
	V8NPH4 ^{F14}	42.76	75.53	4	2	Lysosomal Pro-X carboxypeptidase (<i>Ophiophagus hannah</i>)	Peptidase

¹ The theoretical mass was calculated by subtracting the mass of the signal peptide using the PeptideMass online software. ^{F4, F5, F8–F14} Corresponds to the venom fraction (F) of *O. scutellatus* in which the same protein is present.

Table 2. Identified proteins in the venom of *O. scutellatus* by proteomic analysis.

Fraction	UNIPROT Code	Theoretical Mass (kDa) ¹	−10lgP	Peptides	Unique Peptides	Protein Description	Type
3	Q45Z11	6.73	122.20	6	1	Short neurotoxin 1 (<i>O. scutellatus</i>)	3FTx
4	P0CB06 ^{F4}	6.79	94.79	4	4	Short neurotoxin 2 (<i>O. scutellatus</i>)	3FTx
	A8HDK9	7.89	67.94	5	5	Long neurotoxin 1 (<i>O. scutellatus</i>)	3FTx
5	B7S4N9 ^{F4}	7	142.30	8	7	Kunitz-type serine protease inhibitor taicotoxin (<i>O. scutellatus</i>)	Kunitz
6	P83228	3.66	82.03	3	3	Natriuretic peptide TNP-b (<i>O. scutellatus</i>)	NP

Table 2. Cont.

Fraction	UNIPROT Code	Theoretical Mass (kDa) ¹	−10lgP	Peptides	Unique Peptides	Protein Description	Type
7	Q45Z47	13.33	178.33	14	2	Phospholipase A2 OS2 (<i>O. scutellatus</i>)	PLA ₂
	Q4VRI4	14.2	172.76	14	1	OS6 (<i>O. scutellatus</i>)	PLA ₂
	P10116	13.35	78.09	4	1	Basic phospholipase A2 2 (<i>Laticauda colubrina</i>)	PLA ₂
	A0A898INR6	14.71	71.72	2	1	Phospholipase A (2) (<i>Calliophis bivirgatus</i>)	PLA ₂
8	Q4VRI7 ^{F8}	14.35	157.86	10	5	Alpha taipoxin-2 (<i>O. scutellatus</i>)	PLA ₂
	Q45Z48	14.59	144.13	7	2	PLA-6 (<i>O. scutellatus</i>)	PLA ₂
	A6MFM9	14.52	101.38	3	2	PLA2-4 (<i>Cryptophis nigrescens</i>)	PLA ₂
	P14615	13.42	50.97	2	1	Neutral phospholipase A2 3 (<i>Bungarus fasciatus</i>)	PLA ₂
9	Q45Z45 ^{F10}	15	122.02	7	1	PLA-1 (<i>O. microlepidotus</i>)	PLA ₂
	P00614 ^{F9}	13.83	179.92	13	8	Basic phospholipase A2 taipoxin alpha chain (<i>O. scutellatus</i>)	PLA ₂
	Q4VRI5 ^{F13}	14.1	172.67	11	2	Phospholipase A2 OS1 (<i>O. scutellatus</i>)	PLA ₂
	A6MFM9	14.52	65.31	3	2	PLA2-4 (<i>Cryptophis nigrescens</i>)	PLA ₂
	A8HDK2 ^{F9}	6.34	102.63	4	4	Short neurotoxin 3 (<i>O. scutellatus</i>)	3FTx
	Q3SAX8	4.11	96.42	5	4	Natriuretic peptide OsNP-d (fragment) (<i>O. scutellatus</i>)	NP
10	Q45Z46 ^{F11}	13.33	125.32	8	3	Neutral phospholipase A2 paradoxin-like beta chain (<i>O. microlepidotus</i>)	PLA ₂
	Q45Z51 ^{F10}	14.95	171.88	10	5	PLA-3 (<i>O. scutellatus</i>)	PLA ₂
	Q3HXZ0 ^{F11}	13.39	64.42	3	3	Venom nerve growth factor 2 (<i>O. microlepidotus</i>)	NGF
11	P00615 ^{F11}	13.24	170.01	16	9	Neutral phospholipase A2 homolog taipoxin beta chain 1 (<i>O. scutellatus</i>)	PLA ₂
	P0CG57	13.31	132.04	9	1	Neutral phospholipase A2 homolog taipoxin beta chain 2 (<i>O. scutellatus</i>)	PLA ₂
	Q3I5F4	13.38	99.42	4	4	Venom nerve growth factor (<i>O. scutellatus</i>)	NGF
12	P00616 ^{F12}	44.72	172.56	12	9	Acidic phospholipase A2 homolog taipoxin gamma chain (<i>O. scutellatus</i>)	PLA ₂
	A7X4T2 ^{F9}	6.87	83.17	2	2	Three-finger toxin 3FTx-Oxy6 (<i>O. microlepidotus</i>)	3FTx
	Q58L96	44.69	128.30	6	6	Venom prothrombin activator oscutarin-C catalytic subunit (<i>O. scutellatus</i>)	PTA
	Q3SB07 ^{F11}	23.55	151.14	16	3	Cysteine-rich venom protein pseudochetoxin-like (<i>O. scutellatus</i>)	CRISP
	Q8UW11	24.54	94.05	7	1	Cystein-rich venom protein 2 (<i>Hydrophis hardwickii</i>)	CRISP
13	Q45Z50 ^{F13}	15.21	135.44	5	1	PLA-4 (<i>O. scutellatus</i>)	PLA ₂
	Q58L91	157.79	200.61	34	3	Venom prothrombin activator oscutarin-C non catalytic subunit (<i>O. scutellatus</i>)	PTA

Table 2. Cont.

Fraction	UNIPROT Code	Theoretical Mass (kDa) ¹	−10lgP	Peptides	Unique Peptides	Protein Description	Type
14	A0A670Y1M6 F14	53.81	130.34	12	6	Prolylcarboxypeptidase (<i>Pseudonaja textilis</i>)	Peptidase
	A0A8C6XDV9	54.70	117.08	8	1	Prolylcarboxipeptidase (<i>Naja naja</i>)	Peptidase
	V8NPH4 ^{F14}	42.76	78.45	4	2	Lysosomal Pro-X carboxypeptidase (<i>Ophiophagus hannah</i>)	Peptidase

¹ The theoretical mass was calculated by subtracting the mass of the signal peptide using the PeptideMass software. F4, F8–F14 Corresponds to the venom fraction (F) of *O. microlepidotus* in which the same protein is present.

To confirm the presence of the proteins identified in the proteomic analysis, the crude venom of both snake species was analyzed by MALDI-TOF mass spectrometry. As shown in Figure 4, the mass profiles of *Oxyuranus* venoms are comparable, displaying a range from 3000 *m/z* to 14,000 *m/z*. Most of the proteins identified in the venoms (Tables 1 and 2) present theoretical masses within this range, supporting a correlation between the proteomic identifications and the experimentally observed mass spectra.

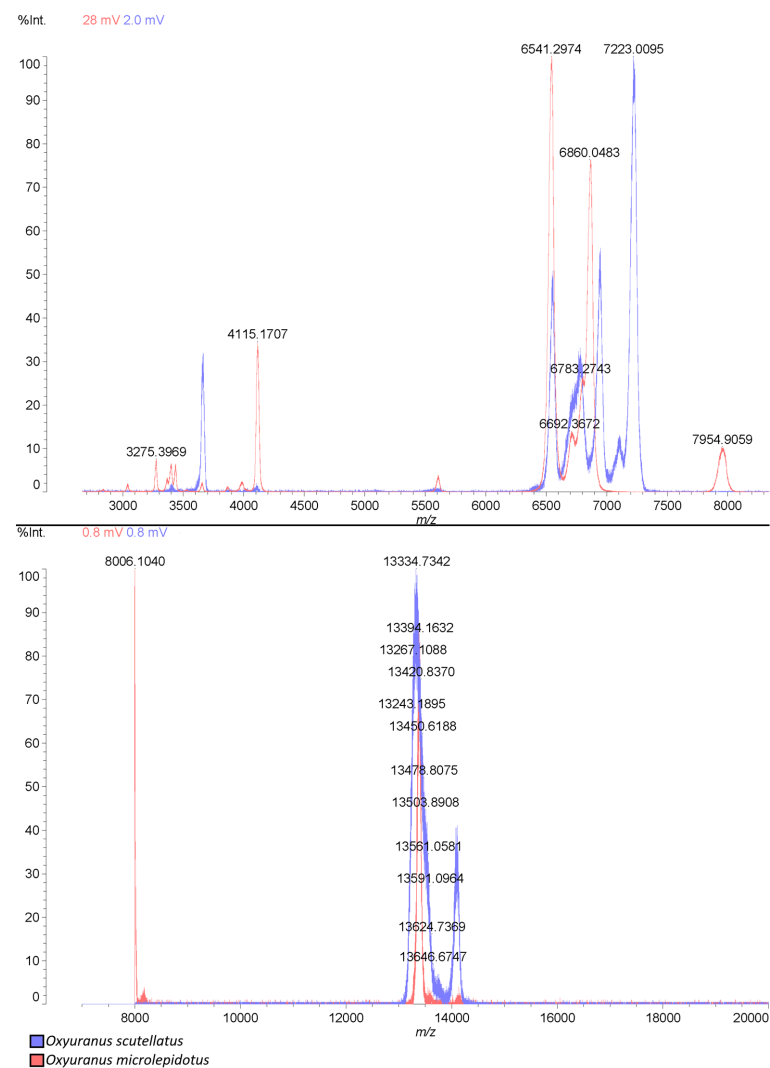


Figure 4. MALDI-TOF spectra from the venoms of *Oxyuranus scutellatus* (blue) and *Oxyuranus microlepidotus* (red).

interactions, conformational stability, and functional properties. Q45Z51, however, closely resembles the reference (pI 4.80), suggesting minimal impact.

nomenclature	uniprot	sequence
Alpha taipoxin-2	Q4VRI7	MHPAHLVLLAVCVSLLGASDIPPLPLNLVQFGFMKCANRNSRPVSHYMDYGCYCGPGG
PLA-5	Q45Z49	MHPAHLVLLAVCVSLLGASDIPPLPLNLVQFGFMIECAIRNRQPALDFMNYGCYCGTVG
Phospholipase A2 OS2	Q45Z47	MHPAHLVLLAVCVSLLGASDIPPLPLNLAQFGFMIRCANGGSRSPLDYTDYGCYCGKGG
PLA-5	Q45Z41	MHPAHLVLLAVCVSLLGASDIPPLPLNLAQFGFMKCANRNSRPVSHYMDYGCYCGKGG
OS6	Q4VRI4	MHPAHLVLLAVCVSLLGASDIPPLPLNLVQFGFMKCANRNSRPVSHYMDYGCYCGKGG
		*****.***.:.:***** *
Alpha taipoxin-2	Q4VRI7	SGTPIDDLDRCCQVHDCYDEAVRRYRCSPLYLTMYSWKCYGTAPSCNSKTQCEGFVCNCD
PLA-5	Q45Z49	CGTPVDDLDRCCQVHDCYGEAEKRLGCSPFVTLYSWKCYGKAPSCNTKTDQC RFVCNCD
Phospholipase A2 OS2	Q45Z47	RGTPVDDLDRCCQVHDCYGEAEKRLGCSPFVTLYSWKCYGKAPSCNTKTDQC RFVCNCD
PLA-5	Q45Z41	SGTPVDELDRCQVHDCYGEAEKRFKCVPFVTLYSWKCYGKAPSCNTKTDQC RFVCNCD
OS6	Q4VRI4	SGTPVDELDRCQVHDCYGEAEKRLGCSPFVTLYSWKCYGKAPSCNTKTDQC RFVCNCD
		:*:**:*.** :* * *:*:*****.*****:**:*: *****
Alpha taipoxin-2	Q4VRI7	AKAAECFARSPYQPSNRNINTKERCK
PLA-5	Q45Z49	AKAAECFARSPYQKKNWNINTKARCK
Phospholipase A2 OS2	Q45Z47	AKAAECFARSPYQKKNWNINTKARCK
PLA-5	Q45Z41	AKAAECFARSPYQKKNWNINTKARCK
OS6	Q4VRI4	AKAAECFARSPYQKKNWNINTKERCK
		*****. * ***** **

Figure 7. ClustalW alignment of OS2-homologous PLA₂s identified in the venoms of *O. scutellatus*: Q4VRI7, Q45Z47 and Q4VRI4, and *O. microlepidotus*: Q4VRI7, Q45Z49 and Q45Z41. OS2 is highlighted in gray. “*” -> fully conserved residues; “:” -> conservative substitution between residues; “.” -> semiconservative substitution between residues. Standard ClustalW color codes used for amino acid polarity/charge.

OS2 homologs exhibit marked residue substitutions that shift their predicted isoelectric points. Q4VRI7 (pI = 7.62) shows extensive changes, including neutral-to-basic (G41R, W137R), acidic-to-basic (D48H), basic-to-neutral (K58P, R61S, R87G, K102T, R114G, K134P, K135P), neutral-to-acidic (G80D, Q113E, A143E), and acidic-to-neutral (E77Q, E83V) substitutions, collectively increasing negative charge compared to OS2 (pI = 8.18). Q45Z49 (pI = 7.57) also harbors key substitutions—basic-to-acidic (R37E), neutral-to-basic (S43R), basic-to-neutral (R44Q, R61C, K58T), and acidic-to-neutral (D51N)—further lowering its pI. In contrast, Q4VRI4 (pI = 7.87) and Q45Z41 (pI = 8.06) share changes such as D48H and R61S, although Q4VRI4 uniquely presents a nonpolar-to-acidic substitution (A143E), rendering Q45Z41 more similar to OS2 in its electrostatic profile.

In the venom of *O. microlepidotus*, the PLA₂ 1 (P60043) was identified, originally characterized from the venom of *Naja sagittifera* [46]. It displays a heterodimeric structure and is calcium-dependent, with Ca²⁺ ions being essential for both its structural stability and catalytic activity on phospholipids. Similarly, PLA₂ 2 (P10116), identified in the venom of *O. scutellatus*, was initially isolated from *Laticauda colubrina*. This enzyme also exhibits Ca²⁺ dependent phospholipase activity, with a reported LD₅₀ of 45 µg/kg [47].

Some PLA₂s identified in this study have not yet been functionally described in the literature; however, they share significant homology with well-characterized proteins. An example is PLA₂ S8-51 (Q9PUH0), a protein which exhibits high sequence similarity to notexin (P00608), as shown in the alignment presented in Figure 8. Notexin, originally isolated from the venom of *Notechis scutatus scutatus*, displays typical phospholipase activity, catalyzing the hydrolysis of phospholipids in muscle or neuronal cell membranes and inhibiting acetylcholine-mediated neurotransmission. Additionally, it has been shown to exert marked nephrotoxic effects in mice following subcutaneous administration, causing glomerular and tubular damage [48,49].

nomenclature	uniprot	sequence
Basic PLA ₂ notexin	P00608	-----NLVQFSYLIQCANHGKRP ^T WHYMDYGCYCGAGG
Acidic PLA ₂ S8-51	Q9PUH0	MYP ^A HLLVLLAVCV ^S LLGAASIPPQPLNLVQFSYLIQCANHGS ^R ATW ^H YTDYGCYCGSGG
		*****:***
Basic PLA ₂ notexin	P00608	SGTPVDELDR ^C CKI ^H DDCYDEAG ^K KGCFPKMSAYD ^Y YCGENGPYCRN ^I KKK ^C LR ^F VCDCD
Acidic PLA ₂ S8-51	Q9PUH0	SGTPVDELDR ^C Q ^T HDN ^C YGEAE ^K KG ^C YPKMSAYD ^Y YCGG ^D GPYCRN ^I R ^K EC ^Q RFV ^C DCD
		*****:***:***:*****:*****:***
Basic PLA ₂ notexin	P00608	VEAA ^F CF ^A KAPYNNAN ^W NI ^D TK ^R RC ^Q
Acidic PLA ₂ S8-51	Q9PUH0	AIAA ^K CF ^A RAPYNDAN ^W DI ^D TET ^R RC ^Q
		. ** ***:***:***:***:***:***

Figure 8. ClustalW alignment of Notexin-homologous PLA₂ identified in the venom of *O. scutellatus*: Q9PUH0. Notexin is highlighted in gray. “*” -> fully conserved residues; “:” -> conservative substitution between residues; “.” -> semiconservative substitution between residues. Standard ClustalW color codes used for amino acid polarity/charge.

Protein Q9PUH0 exhibits structural features that distinguish it from notexin. A key difference is the greater prevalence of acidic residues, arising from multiple substitutions: basic-to-neutral (K16S43, K46Q73, K116T143), basic-to-acidic (K84E111, K115E142), neutral-to-acidic (G56E83, N74D101, N107D134, N111D138), neutral-to-basic (F98K125), and acidic-to-neutral (D50N77, D53G80, E73G100, E95I122). Collectively, these changes lower its predicted isoelectric point (Q9PUH0: pI = 5.08 vs. notexin: pI = 7.39). Such alterations may influence electrostatic intramolecular interactions, potentially impacting protein stability and conformation.

PLA₂ accounted for approximately 47% of the proteins identified in *O. microlepidotus* (Figure 2), and about 66% of the proteins in *O. scutellatus* (Figure 2), indicating a higher relative abundance of this type of toxin in *O. scutellatus* venom.

2.3. Three-Fingers Toxins (3FTx)

Among the identified protein families, three-finger toxins (3FTxs) represent one of the most relevant groups in taipan venoms, given their abundance, structural versatility, and central role in neurotoxicity, the 3FTX were identified in both venoms (Tables 1 and 2). 3FTx are peptides consisting of approximately 60 to 74 amino acid residues and are found in various snake families. Their structure is composed of three beta-sheet loops connected to a central core, forming a three-dimensional conformation that resembles three fingers, hence the name [50]. These toxins are highly potent, acting through interaction with acetylcholine receptors (AChRs), where they block the action of acetylcholine, leading to inhibition of neurotransmission at the neuromuscular junction and, consequently, to paralysis [51].

As observed with PLA₂, a greater diversity of 3FTx was identified in the venom of *O. microlepidotus*, accounting approximately 33% of the identified proteins (Figure 2), compared to about 9% of the identified protein composition in *O. scutellatus* venom (Figure 2).

The toxin SNTX-1 (Q45Z11) found in the venom of *O. scutellatus* was described by Zamudio et al. [52]. According to the authors, this toxin exhibits a high inhibitory capacity on skeletal muscle AChRs, with an IC₅₀ of 2.4 ± 0.4 nM. In contrast, it does not display the same affinity for brain AChRs, suggesting a postsynaptic site of action. The authors also described SNTX-2 (P0CB06), identified in the venom of both snake species. This 3FTx exhibits a mode of action similar to that of SNTX-1. Although SNTX-1 itself was not identified in the venom of *O. microlepidotus*, a homologous protein, named 3FTx-Oxy4 (A7X4S0) was detected. The sequence alignment is shown in Figure 9.

nomenclature	uniprot	sequence
SNTX-1	Q45Z11	MKTL LL TLV V VTIVCLDLGY TM TCYNQ QS SEAKTTTTCSSGGVSSCYK KT WSDGRG TI IER
Short neurotoxin 3FTx-Oxy4	A7X4S0	MKTL LL TLV V VTIVCLDLGY TM TCYNQ QS SEAKTTTTCSSGGVSSCYK ET WYDGRG TR IER *****:*** **
SNTX-1	Q45Z11	GCGCPSVKKGIERIC CR TDKCNN
Short neurotoxin 3FTx-Oxy4	A7X4S0	GCGCPRAKKGIERIC CG TDKCNN *****.***** **

Figure 9. ClustalW alignment of SNTX-1-homologous 3FTx identified in the venom of *O. microlepidotus*: A7X4S0. SNTX-1 is highlighted in gray. “*” -> fully conserved residues; “:” -> conservative substitution between residues; “.” -> semiconservative substitution between residues. Standard ClustalW color codes used for amino acid polarity/charge.

Three proteins identified in the venom of *O. microlepidotus* (A7X4R0; A8HDK8; A7X4Q3) and one protein identified in the venom of *O. scutellatus* (A8HDK9) show sequence homology to a well-characterized 3FTx, Elapitoxin-Oh3a (Q53B58). The alignment of these sequences is presented in Figure 10. This toxin was shown to induce blockade of nerve stimulation in the biventer cervicis muscle of chickens when challenged with endogenous acetylcholine and carbachol (CCh), both of which activate muscarinic and nicotinic receptors [53]. The authors also suggested a pseudo-irreversible antagonistic effect of this toxin based on a concentration-dependent, non-parallel rightward shift in the cumulative concentration-response to CCh, accompanied by a reduction in the maximal response in unstimulated chick muscle. However, this effect was not observed upon stimulation with KCl, further supporting a postsynaptic site of action for this toxin.

nomenclature	uniprot	sequence
Alpha elapitoxin Oh3a	Q53B58	MKTL LL TLV V VTIVCLDLGY TT KCYVTPDVK SET CPAGQDICY ET WCD AW CTSRG KRV N
Long neurotoxin 3FTx-Oxy2	A7X4R0	MKTL LL TLV V VTIVCLDLGY TR RCFTTPSV R SERC PP GQEV CY TKT WT DGHG SR GK RV D
Long neurotoxin 1	A8HDK9	MKTL LL TLV V VTIVCLDLGY TR RCFTTPSV R SERC PP GQEV CY TKT WT DGHG SR GK RV D
Long neurotoxin 2	A8HDK8	MKTL LL TLV V VTIVCLDLGY TR RCFITP D VRSER C PPGQEV CY TKT W CDG F CSSR G K RV D
Long neurotoxin 3FTx-Oxy1	A7X4Q3	MKTL LL TLV V VTIVCLDLGY TR RCFITP D VRSER C PPGQEV CY TKT W CDG F CSSR G K RV D *****:*** **
Alpha elapitoxin Oh3a	Q53B58	LGCAATCPIVK-PGVEIKCCST D NCNPF P TRKRP
Long neurotoxin 3FTx-Oxy2	A7X4R0	LGCAATCPTPKKKIKI IC CSK D NCN T FPKWP--
Long neurotoxin 1	A8HDK9	LGCAATCPTPKKKIKI IC CSK D NCN T FPKWP--
Long neurotoxin 2	A8HDK8	LGCAATCPTPKKKGID I IC S K D NCN T FPKWP--
Long neurotoxin 3FTx-Oxy1	A7X4Q3	LGCAATCPTPKKKGID I IC S K D NCN T FPKWP-- ***** * .:. ***.*** **.

Figure 10. ClustalW alignment of Elapitoxin-Oh3a-homologous 3FTx identified in the venoms of *O. microlepidotus*: A7X4R0, A8HDK8 and A7X4Q3, and *O. scutellatus*: A8HDK9. Elapitoxin-Oh3a is highlighted in gray. “*” -> fully conserved residues; “:” -> conservative substitution between residues; “.” -> semiconservative substitution between residues. Standard ClustalW color codes used for amino acid polarity/charge.

3FTx possess particularly relevant characteristics for studies targeting molecular mechanisms related to pain modulation. A series of 3FTxs with inhibitory action on acid-sensing ion channels (ASICs) has been characterized from the venom of the snake *Dendroaspis polylepis*, resulting in analgesic effects comparable to those of morphine [54]. Interestingly, some proteins identified in the venom of *O. microlepidotus* show a degree of sequence homology with one of the characterized 3FTx, mambalgin-1 (P0DKR6). The alignment of these sequences is presented in Figure 11.

ASICs are expressed in both the central and peripheral nervous systems (especially in nociceptive neurons) and play a key role in signaling and propagation of pain [55]. For this reason, the inhibition of these channels by 3FTx is directly associated with the induction of analgesia.

nomenclature	uniprot	sequence
Mambalgin-1	PODKR6	MKTL LL LLVVTIVCLDLGYSLKCYQH G ---KVV T CHRDMKFCYHNTGMPFRNLKLILQ G
Three-finger toxin 3FTx-Oxy6	A7X4T2	MKTL LL SLVVM T IVYLDLGYTLKCHESENLDHVVCEEDE T MCYKFTFV P FRDFEIVARG
Toxin 3FTx-Oxy5	A7X4S7	MKTL LL TLVVM T IVCLDLGYTLTCYMN--PSG T MVCKEHE T MCYRLIVWTFQYHVLYLKG
Short neurotoxin 3	A8HDK2	MKTL LL TLVVM T IVCLDLGYTLTCYMN--PSG T MVCKEHE T MCYQLIVWTFQYRVLYLKG
		*****:*:*:*:* *****:*:*: :.*... ::*:* *:* : :*
Mambalgin-1	PODKR6	CS S SC S ETEN N KCC S TDR C NK
Three-finger toxin 3FTx-Oxy6	A7X4T2	CS A SC P EEK D VVCC S TDL C NK
Toxin 3FTx-Oxy5	A7X4S7	CS S SC P GG N NCACC S TDL C NN
Short neurotoxin 3	A8HDK2	CT S SC P GG N NRACC S TDL C NN
		::* *:* ***** *:*

Figure 11. ClustalW alignment of Mambalgin-1-homologous 3FTxs identified in the venom of *O. microlepidotus*: A7X4T2, A7X4S7 and A8HDK2. Mambalgin-1 is highlighted in gray. “*”-> fully conserved residues; “:”-> conservative substitution between residues; “.”-> semiconservative substitution between residues. Standard ClustalW color codes used for amino acid polarity/charge.

Recent studies have also revealed that ASICs are involved in processes within the central nervous system related to the release of neurotransmitters such as GABA and glutamate, and are implicated in pathophysiological mechanisms associated with neurological disorders such as epilepsy and Alzheimer’s disease [56,57]. These findings make 3FTxs promising targets for therapeutic investigations in neuroscience.

2.4. Other Proteins

In addition to the dominant toxin families, several other protein groups were identified in the venoms of *O. microlepidotus* and *O. scutellatus* (Tables 1 and 2). Nerve growth factors (NGFs) accounted for ~1.45% and ~4.10% of proteins, respectively (Figure 2). Despite limited characterization of the sequences detected (Q3HXZ0; Q3I5F4), they show homology with NGF (Supplementary Figure S1) from *Macrovipera lebetinus* (P25428), previously reported to stimulate neurite outgrowth in PC12 cells [55,58–63]. Such findings reinforce the widespread presence of NGFs in snake venoms and their potential role beyond neuronal regulation, including tissue repair and neuroinflammatory processes. Prothrombin activators (PTAs) were also detected (~0.82% in *O. microlepidotus* and ~1.98% in *O. scutellatus*), with Oscutarin-C (Q58L96; Q58L91) identified in *O. scutellatus* as a potent procoagulant toxin, and the homolog Omicarin-C (Q58L95) present in *O. microlepidotus* (Supplementary Figure S2) [22,64–69].

Natriuretic peptides (NPs) constituted one of the most abundant protein classes among this group, reaching ~14.57% in *O. microlepidotus* and ~7.41% in *O. scutellatus*. Functional differences were observed, as TNP-b (P83228) from *O. scutellatus* exhibited reduced vasorelaxant activity and failed to activate the GC-A receptor, while homologs of TNP-c (Q3SAF8; Q3SAX8) (Supplementary Figure S3) identified in both species displayed potent vasodilatory effects [70–76]. These peptides resemble mammalian NPs in structure and activity, suggesting their involvement in prey immobilization via hypotension and highlighting their potential as templates for cardiovascular drug discovery. CRISPs were also identified, in smaller proportions (~0.58% and ~2.34%), including homologs such as pseudocin (Supplementary Figure S4), known to inhibit cyclic nucleotide-gated channels but with limited direct toxicity [77–84]. Notably, CRISPs have been associated with anti-angiogenic and antiparasitic activities in other species, expanding their relevance beyond envenomation.

Kunitz-type inhibitors added further diversity, with taicatoxin (B7S4N9) present in both venoms (~0.37% in *O. microlepidotus* and ~5.69% in *O. scutellatus*), acting as a heterotrimeric complex that blocks cardiac CaV channels [18,19,85–92]. In addition to classical protease inhibition, Kunitz toxins have been reported to modulate ion channels and display pharmacological properties, including AVP antagonism, anti-angiogenic, and anticoagulant

activities [93–96]. Finally, carboxypeptidases (~0.74% and ~2.46%) were identified in both venoms (Figure 2). Although scarcely studied in snakes, these enzymes are known to cleave peptides at the carboxy-terminal end, participate in angiotensin regulation, coagulation, and inflammatory pathways [97,98]. Taken together, these protein families highlight the functional complexity of taipan venoms, extending their biological impact beyond neurotoxicity and supporting their potential as valuable models for biomedical applications.

3. Conclusions

Both *Oxyuranus* venoms exhibit a shared proteomic framework dominated by PLA₂s and 3FTxs, yet a clear divergence in toxin repertoire highlights distinct functional strategies. While *O. scutellatus* venom appears predominantly PLA₂-driven, reinforcing its role in presynaptic neurotoxicity and myotoxicity, *O. microlepidotus* displays an expanded diversity of 3FTxs coupled with the exclusive presence of 5'-nucleotidases and Waprin, indicating a broader range of neurotoxic and cardiocirculatory mechanisms. These compositional differences suggest evolutionary pressures that may underlie the greater lethality historically attributed to *O. microlepidotus*, potentially reflecting ecological adaptation through diversification of effector molecules. The identification of Waprin, alongside several uncharacterized proteins, not only broadens the functional scope of taipan venoms but also emphasizes their unexplored pharmacological potential, positioning them as valuable resources for future studies on toxin evolution, molecular mechanisms of envenomation, and the discovery of novel therapeutic leads.

4. Materials and Methods

4.1. Venom Fractioning

The lyophilized venoms of *O. microlepidotus* and *O. scutellatus* (3 mg each), provided by Venom Supplies (Tanunda, SA) were resuspended in 0.1% Trifluoroacetic Acid (TFA) and centrifuged (10,000 × g) for 10 min, at 4 °C. The supernatant was then fractionated by reversed-phase high-performance liquid chromatography (RP-HPLC) in a Shimadzu Prominence binary system (Shimadzu, Kyoto, Japan), coupled to a C18 analytical column (250 mm × 4.6 mm, 5 μm). UV detection was performed (SPDM 20A, Shimadzu, λ = 214 nm) and separation was achieved by a linear gradient of 20–100% solvent B (90% acetonitrile, containing 0.1% TFA) over A (0.1% TFA) for 50 min at a constant flow of 1 mL·min⁻¹. The use of this strategy aimed to enhance the resolution for fractionation, and later proteomic analysis, thereby enabling more precise identification and characterization of the venom constituents.

4.2. Fractions Characterization

4.2.1. Protein Digestion

The collected fractions (50 μL aliquots) were digested with trypsin (Sigma-Aldrich, St. Louis, MO, USA) following a standardized protocol. Initially, samples were buffed in 50 mM ammonium bicarbonate diluted in water and reduced with 5 μL of 100 mM dithiothreitol (DTT) at 60 °C for 30 min. Alkylation was performed using 5 μL of 100 mM iodoacetamide (IAA) in the dark for 45 min. Subsequently, enzymatic digestion was carried out with 240 ng of sequencing-grade trypsin at 30 °C for 16 h. Trypsin activity was quenched by the addition of 5 μL of 10% TFA, and the resulting peptide mixtures were stored at −20 °C until LC-MS/MS analysis.

4.2.2. Analysis by LC-ESI-IT-TOF/MS

The samples then were analyzed with liquid chromatography mass spectrometry in an ESI-IT-TOF instrument coupled to a UPLC 20A Prominence (Shimadzu, Kyoto, Japan). Sam-

ples (50 μ L aliquots) were loaded into a C18 column (Kinetex C18, 5 μ m; 50 mm \times 2.1 mm) and fractionated by a binary gradient employing as solvents (A) water:acetic acid (999:1) and (B) ACN:water:acetic acid (949:50:1). An elution gradient of 0–40% B was applied for 80 min at a constant flow of 0.2 mL·min⁻¹ after initial isocratic elution for 5 min. The eluates were monitored using a Shimadzu SPD-M20A PDA detector before being injected into the mass spectrometer.

The interface was kept at 4.5 kV and 200 °C. The detector operated at 1.95 kV and the argon collision induced fragmentation was set at 55 ‘energy’ value. MS spectra were acquired in positive mode in the 350–1400 m/z range, and MS/MS spectra were collected in the 50–1950 m/z range.

4.2.3. Analysis by MALDI-TOF/MS

The venoms were also analyzed using a matrix-assisted laser desorption ionization-time of flight (MALDI-TOF) mass spectrometer (Axima Performance, Shimadzu, Kyoto, Japan). One microliter of each sample was co-crystallized with 1 μ L of α -cyano-4-hydroxycinnamic acid matrix (Sigma-Aldrich, St. Louis, MO, USA) for the low m/z range (1000~10,000) and with 1 μ L of 3,5-dimethoxy-4-hydroxycinnamic acid (Sigma-Aldrich, St. Louis, MO, USA) for the high m/z range (8000~20,000). The plate containing the samples was then dried at room temperature. The mass spectrum was obtained in linear positive mode.

4.2.4. Proteomic Data Processing and Data Analysis

Raw LCD Shimadzu datafiles were converted into mzML files using the LCMSolution tool and then loaded into Peaks Studio V7.0 (Bioinformatic Solutions Inc., Waterloo, ON, Canada). Data were processed according to the following parameters: MS and MS/MS error mass were 0.1 Da; methionine oxidation and carbamidomethylation as variable and fixed modification, respectively; trypsin as cleaving enzyme; maximum missed cleavages (3), maximum variable PTMs per peptide (3), and non-specific (1). Data were analyzed against the “Snakes” database, compiled in December/2024 by UNIPROT. Only peptides with a $-10\log P$ (20) and proteins with a $-10\log P$ (20), containing at least one unique peptide, were considered in the analyses. Protein alignment was performed by Clustal Omega (v. 1.2.4) (EMBL-EBI). The theoretical mass was calculated by subtracting the mass of the signal peptide using the PeptideMass software (https://web.expasy.org/peptide_mass/, accessed on 26 August 2025).

4.2.5. Quantitative Analysis of Venom Proteins

The quantitative analysis of venom proteins was performed based following the approach described by Beraldo-Neto (2023) [99]: Quantification was based on the area under the chromatographic peaks, as calculated using LCMSolution software (v 1.25), and used as a proxy for protein abundance. In cases where multiple proteins co-eluted within the same retention time (i.e., within the same fraction), the relative contribution of each protein to the total peak area was estimated by normalizing the number of unique peptides identified for each protein.

4.3. Computational Pocket Mapping

We used the Deep Origin platform (Balto module) to perform automated binding pocket detection and characterization on the B5G6G7 (Omwaprin-b) structure. First, the input PDB file was cleaned and preprocessed (e.g., removal of water molecules, addition of missing atoms, protonation at physiological pH) through the built-in protein preparation routines. Next, the platform’s pocket-finding algorithm was invoked to scan the protein surface for putative ligand-binding cavities. Deep Origin exposes a Pocket class

within its pipeline (via `deeporigin.drug_discovery.Pocket`) that supports operations such as `from_pdb_file`, `from_pocket_finder_results`, and `get_center`, enabling extraction of pocket geometry and coordinate data. client-docs.deeporigin.io.

Once pockets were detected, the system computed a panel of pocket descriptors including volume, hydrophobicity, polarity, total solvent-accessible surface area (SASA), and drugability score. These metrics are drawn from internal scoring models that integrate physical and statistical features (e.g., topology, atom types, hydrophobic patches) to estimate drug-likeness. The pocket center coordinates were derived by averaging the atomic positions within the cavity (via the `get_center()` method). The default docking grid box size (24 Å) was applied around the pocket center for further docking and validation procedures. After annotation, the highest-scoring pocket (“Red Pocket”) was selected for downstream mechanistic interpretation and binding modeling.

Supplementary Materials: The following supporting information can be downloaded at: <https://www.mdpi.com/article/10.3390/toxins17100488/s1>, Figure S1: ClustalW alignment of NGF-homologous NGF identified in the venoms of *O. microlepidotus*: Q3HXZ0, and *O. scutellatus*: Q3HXZ0 and Q3I5F4. NGF is highlighted in gray. “*” -> fully conserved residues; “:” -> conservative substitution between residues; “.” -> semiconservative substitution between residues. Standard ClustalW color codes used for amino acid polarity/charge; Figure S2: ClustalW alignment of Oscutarin-C-homologous VPTA identified in the venom of *O. microlepidotus*: Q58L95. Oscutarin-C is highlighted in gray. “*” -> fully conserved residues; “:” -> conservative substitution between residues; “.” -> semiconservative substitution between residues. Standard ClustalW color codes used for amino acid polarity/charge. Figure S3: ClustalW alignment of TNP-c-homologous NP identified in the venom of *O. microlepidotus*: Q3SAF8 and Q3SAX8. TNP-c is highlighted in gray. “*” -> fully conserved residues; “:” -> conservative substitution between residues; “.” -> semiconservative substitution between residues. Standard ClustalW color codes used for amino acid polarity/charge. Figure S4: ClustalW alignment of Pseudecin-homologous CRISPs identified in the venoms of *O. microlepidotus*: Q3SB07, and *O. scutellatus*: Q3SB07 and Q8UW11. Pseudecin is highlighted in gray. “*” -> fully conserved residues; “:” -> conservative substitution between residues; “.” -> semiconservative substitution between residues. Standard ClustalW color codes used for amino acid polarity/charge.

Author Contributions: Conceptualization, G.G.P. and E.B.-N.; writing—original draft preparation, G.G.P.; writing—review and editing, E.B.-N. and P.J.S.; supervision and funding acquisition, D.C.P. and E.B.-N. All authors have read and agreed to the published version of the manuscript.

Funding: This research was funded by Butantan Foundation grant number 001/0708/000.590/2023 and 001/0708/000.126/2025 to DCP; FAPESP Grant 2024/10962-9 and 2022/11535-1; DCP is a National Council for Scientific and Technological Development (CNPq) fellow (305525/2023-9).

Institutional Review Board Statement: Not applicable.

Informed Consent Statement: Not applicable.

Data Availability Statement: The proteomic data presented in this study are available on request from the corresponding author due to the confidentiality clauses reason.

Conflicts of Interest: The authors declare no conflicts of interest.

References

1. Hardy, M.C.; Cochrane, J.; Allavena, R.E. Venomous and poisonous Australian animals of veterinary importance: A rich source of novel therapeutics. *BioMed Res. Int.* **2014**, *2014*, 671041. [[CrossRef](#)] [[PubMed](#)]
2. Williams, D.; Wüster, W.; Fry, B.G. The good, the bad and the ugly: Australian snake taxonomists and a history of the taxonomy of Australia’s venomous snakes. *Toxicon* **2006**, *48*, 919–930. [[CrossRef](#)]
3. Jackson, T.N.W.; Sunagar, K.; Undheim, E.A.B.; Koludarov, I.; Chan, A.H.C.; Sanders, K.; Ali, S.A.; Hendrikx, I.; Dunstan, N.; Fry, B.G. Venom down under: Dynamic evolution of Australian elapid snake toxins. *Toxins* **2013**, *5*, 2621–2655. [[CrossRef](#)]

4. Kocholaty, W.F.; Ledford, E.B.; Daly, J.G.; Billings, T.A. Toxicity and some enzymatic properties and activities in the venoms of Crotalidae, Elapidae and Viperidae. *Toxicon* **1971**, *9*, 131–138. [[CrossRef](#)]
5. Doughty, P.; Maryan, B.; Donnellan, S.C.; Hutchinson, M.N. A new species of taipan (Elapidae: *Oxyuranus*) from central Australia. *Zootaxa* **2007**, *1422*, 45–58. [[CrossRef](#)]
6. Kornhauser, R.; Hart, A.J.; Reeve, S.; Smith, A.I.; Fry, B.G.; Hodgson, W.C. Variations in the pharmacological profile of post-synaptic neurotoxins isolated from the venoms of the Papuan (*Oxyuranus scutellatus canni*) and coastal (*Oxyuranus scutellatus scutellatus*) taipans. *Neurotoxicology* **2010**, *31*, 239–243. [[CrossRef](#)]
7. Laloo, D.G.; Trevett, A.J.; Korinhona, A.; Nwokolo, N.; Laurenson, I.F.; Paul, M.; Black, J.; Naraqi, S.; Mavo, B.; Saweri, A. Snakebites by the Papuan taipan (*Oxyuranus scutellatus canni*): Paralysis, hemostatic and electrocardiographic abnormalities, and effects of antivenom. *Am. J. Trop. Med. Hyg.* **1995**, *52*, 525–531. [[CrossRef](#)] [[PubMed](#)]
8. Barber, C.M.; Madaras, F.; Turnbull, R.K.; Morley, T.; Dunstan, N.; Allen, L.; Kuchel, T.; Mirtschin, P.; Hodgson, W.C. Comparative studies of the venom of a new Taipan species, *Oxyuranus temporalis*, with other members of its genus. *Toxins* **2014**, *6*, 1979–1995. [[CrossRef](#)] [[PubMed](#)]
9. Crachi, M.T.; Hammer, L.W.; Hodgson, W.C. The effects of antivenom on the in vitro neurotoxicity of venoms from the taipans *Oxyuranus scutellatus*, *Oxyuranus microlepidotus* and *Oxyuranus scutellatus canni*. *Toxicon* **1999**, *37*, 1771–1778. [[CrossRef](#)]
10. Brennan, K.E.C.; Morley, T.; Hutchinson, M.; Donnellan, S. Redescription of the western desert taipan, *Oxyuranus temporalis* (Serpentes: Elapidae), with notes on its distribution, diet and genetic variation. *Aust. J. Zool.* **2011**, *59*, 227. [[CrossRef](#)]
11. Johnston, C.I.; Ryan, N.M.; O’Leary, M.A.; Brown, S.G.A.; Isbister, G.K. Australian taipan (*Oxyuranus* spp.) envenoming: Clinical effects and potential benefits of early antivenom therapy—Australian Snakebite Project (ASP-25). *Clin. Toxicol.* **2017**, *55*, 115–122. [[CrossRef](#)] [[PubMed](#)]
12. Williams, D.; Bal, B. Papuan Taipan (*Oxyuranus scutellatus canni*) envenomation in rural Papua New Guinea. *Ann. ACTM Int. J. Trop. Travel Med.* **2003**, *4*, 6–9.
13. Su, M.J.; Chang, C.C. Presynaptic effects of snake venom toxins which have phospholipase A₂ activity (beta-bungarotoxin, taipoxin, crotoxin). *Toxicon* **1984**, *22*, 631–640. [[CrossRef](#)] [[PubMed](#)]
14. Tzeng, M.C.; Yen, C.H.; Hseu, M.J.; Tseng, C.C.; Tsai, M.D.; Dupureur, C.M. Binding proteins on synaptic membranes for crotoxin and taipoxin, two phospholipases A₂ with neurotoxicity. *Toxicon* **1995**, *33*, 451–457. [[CrossRef](#)] [[PubMed](#)]
15. Fathi, B.; Harvey, A.L.; Rowan, E.G. The effect of temperature on the effects of the phospholipase A neurotoxins beta-bungarotoxin and taipoxin at the neuromuscular junction. *Toxicon* **2013**, *70*, 86–89. [[CrossRef](#)]
16. Treppmann, P.; Brunk, I.; Afube, T.; Richter, K.; Ahnert-Hilger, G. Neurotoxic phospholipases directly affect synaptic vesicle function. *J. Neurochem.* **2011**, *117*, 757–764. [[CrossRef](#)]
17. Harris, J.B.; Maltin, C.A. Myotoxic activity of the crude venom and the principal neurotoxin, taipoxin, of the Australian taipan, *Oxyuranus scutellatus*. *Br. J. Pharmacol.* **1982**, *76*, 61–75. [[CrossRef](#)]
18. Possani, L.D.; Martin, B.M.; Yatani, A.; Mochca-Morales, J.; Zamudio, F.Z.; Gurrola, G.B.; Brown, A.M. Isolation and physiological characterization of taicatoxin, a complex toxin with specific effects on calcium channels. *Toxicon* **1992**, *30*, 1343–1364. [[CrossRef](#)]
19. Earl, S.T.H.; Richards, R.; Johnson, L.A.; Flight, S.; Anderson, S.; Liao, A.; de Jersey, J.; Masci, P.P.; Lavin, M.F. Identification and characterisation of Kunitz-type plasma kallikrein inhibitors unique to *Oxyuranus* sp. snake venoms. *Biochimie* **2012**, *94*, 365–373. [[CrossRef](#)]
20. Su, M.C.; Lee, S.Y.; Tan, C.T.; Su, C.C.; Li, S.Y.; Lin, R.H.; Hung, C.C.; Lin, M.J. Taicatoxin inhibits the calcium-dependent slow motility of mammalian outer hair cells. *Hear. Res.* **2005**, *203*, 172–179. [[CrossRef](#)]
21. Rouault, M.; Rash, L.D.; Escoubas, P.; Boilard, E.; Bollinger, J.; Lomonte, B.; Maurin, T.; Guillaume, C.; Canaan, S.; Deregnacourt, C.; et al. Neurotoxicity and other pharmacological activities of the snake venom phospholipase A₂ OS₂: The N-terminal region is more important than enzymatic activity. *Biochemistry* **2006**, *45*, 5800–5816. [[CrossRef](#)]
22. Herrera, M.; Fernández, J.; Vargas, M.; Villalta, M.; Segura, Á.; León, G.; Angulo, Y.; Paiva, O.; Matainaho, T.; Jensen, S.D.; et al. Comparative proteomic analysis of the venom of the taipan snake, *Oxyuranus scutellatus*, from Papua New Guinea and Australia: Role of neurotoxic and procoagulant effects in venom toxicity. *J. Proteom.* **2012**, *75*, 2128–2140. [[CrossRef](#)]
23. St Pierre, L.; Fischer, H.; Adams, D.J.; Schenning, M.; Lavidis, N.; de Jersey, J.; Masci, P.P.; Lavin, M.F. Distinct activities of novel neurotoxins from Australian venomous snakes for nicotinic acetylcholine receptors. *Cell. Mol. Life Sci.* **2007**, *64*, 2829–2840. [[CrossRef](#)]
24. Fry, B.G.; Wickramaratana, J.C.; Lemme, S.; Beuve, A.; Garbers, D.; Hodgson, W.C.; Alewood, P. Novel natriuretic peptides from the venom of the inland taipan (*Oxyuranus microlepidotus*): Isolation, chemical and biological characterization. *Biochem. Biophys. Res. Commun.* **2005**, *327*, 1011–1015. [[CrossRef](#)]
25. Morrison, J.; Pearn, J.; Covacevich, J.; Tanner, C.; Coulter, A. Studies on the venom of *Oxyuranus microlepidotus*. *J. Toxicol. Clin. Toxicol.* **1983**, *21*, 373–385. [[CrossRef](#)]
26. Broad, A.J.; Sutherland, S.K.; Coulter, A.R. The lethality in mice of dangerous Australian and other snake venom. *Toxicon* **1979**, *17*, 661–664. [[CrossRef](#)]

27. Tasoulis, T.; Silva, A.; Veerati, P.C.; Baker, M.; Hodgson, W.C.; Dunstan, N.; Isbister, G.K. Intra-Specific Venom Variation in the Australian Coastal Taipan *Oxyuranus scutellatus*. *Toxins* **2020**, *12*, 485. [[CrossRef](#)] [[PubMed](#)]
28. van Thiel, J.; Alonso, L.L.; Slagboom, J.; Dunstan, N.; Wouters, R.M.; Modahl, C.M.; Vonk, F.J.; Jackson, T.N.W.; Kool, J. Highly Evolvable: Investigating Interspecific and Intraspecific Venom Variation in Taipans (*Oxyuranus* spp.) and Brown Snakes (*Pseudonaja* spp.). *Toxins* **2023**, *15*, 74. [[CrossRef](#)] [[PubMed](#)]
29. Torres, A.M.; Wong, H.Y.; Desai, M.; Moochhala, S.; Kuchel, P.W.; Kini, R.M. Identification of a novel family of proteins in snake venoms. *J. Biol. Chem.* **2003**, *278*, 40097–40104. [[CrossRef](#)]
30. Wilkinson, T.S.; Roghanian, A.; Simpson, A.J.; Sallenave, J.M. WAP domain proteins as modulators of mucosal immunity. *Biochem. Soc. Trans.* **2011**, *39*, 1409–1415. [[CrossRef](#)] [[PubMed](#)]
31. Nair, D.G.; Fry, B.G.; Alewood, P.; Kumar, P.P.; Kini, R.M. Antimicrobial activity of omwaprin, a new member of the Waprin family of snake venom proteins. *Biochem. J.* **2007**, *402*, 93–104. [[CrossRef](#)]
32. Thankappan, B.; Angayarkanni, J. Biological characterization of omw1 and omw2: Antimicrobial peptides derived from omwaprin. *3 Biotech* **2019**, *9*, 295. [[CrossRef](#)] [[PubMed](#)]
33. Dhananjaya, B.L.; D'Souza, C.J.M. The pharmacological role of nucleotidases in snake venoms. *Cell Biochem. Funct.* **2010**, *28*, 171–177. [[CrossRef](#)]
34. Samel, M.; Vija, H.; Kurvet, I.; Künnis-Beres, K.; Trummal, K.; Subbi, J.; Kahru, A.; Siigur, J. Interactions of PLA₂-s from *Vipera lebetina*, *Vipera berus berus* and *Naja naja oxiana* venom with platelets, bacterial and cancer cells. *Toxins* **2013**, *5*, 203–223. [[CrossRef](#)] [[PubMed](#)]
35. Zieler, H.; Keister, D.B.; Dvorak, J.A.; Ribeiro, J.M. A snake venom phospholipase A₂ blocks malaria parasite development in the mosquito midgut by inhibiting ookinete association with the midgut surface. *J. Exp. Biol.* **2001**, *204*, 4157–4167. [[CrossRef](#)] [[PubMed](#)]
36. Gebrim, L.C.; Marcussi, S.; Menaldo, D.L.; de Menezes, C.S.R.; Nomizo, A.; Hamaguchi, A.; Silveira-Lacerda, E.P.; Homsí Brandeburgo, M.I.; Sampaio, S.V.; Soares, A.M.; et al. Antitumor effects of snake venom chemically modified Lys49 phospholipase A₂-like BthTX-I and a synthetic peptide derived from its C-terminal region. *Biologicals* **2009**, *37*, 222–229. [[CrossRef](#)] [[PubMed](#)]
37. Fohlman, J.; Eaker, D.; Karlsoon, E.; Thesleff, S. Taipoxin, an extremely potent presynaptic neurotoxin from the venom of the Australian snake taipan (*Oxyuranus s. scutellatus*). Isolation, characterization, quaternary structure and pharmacological properties. *Eur. J. Biochem.* **1976**, *68*, 457–469. [[CrossRef](#)]
38. Cendron, L.; Mičetić, I.; Polverino de Laureto, P.; Paoli, M. Structural analysis of trimeric phospholipase A₂ neurotoxin from the Australian taipan snake venom. *FEBS J.* **2012**, *279*, 3121–3135. [[CrossRef](#)]
39. Harrison, J.A.; Aquilina, J.A. Insights into the subunit arrangement and diversity of paradoxin and taipoxin. *Toxicon* **2016**, *112*, 45–50. [[CrossRef](#)]
40. Hodgson, W.C.; Dal Belo, C.A.; Rowan, E.G. The neuromuscular activity of paradoxin: A presynaptic neurotoxin from the venom of the inland taipan (*Oxyuranus microlepidotus*). *Neuropharmacology* **2007**, *52*, 1229–1236. [[CrossRef](#)]
41. Apel, A.R.; Hoban, K.; Chuartzman, S.; Tonikian, R.; Sidhu, S.; Schuldiner, M.; Wendland, B.; Prosser, D. Syp1 regulates the clathrin-mediated and clathrin-independent endocytosis of multiple cargo proteins through a novel sorting motif. *Mol. Biol. Cell* **2017**, *28*, 2434–2448. [[CrossRef](#)]
42. Oishi, Y.; Arakawa, T.; Tanimura, A.; Itakura, M.; Takahashi, M.; Tajima, Y.; Mizoguchi, I.; Takuma, T. Role of VAMP-2, VAMP-7, and VAMP-8 in constitutive exocytosis from HSY cells. *Histochem. Cell Biol.* **2006**, *125*, 273–281. [[CrossRef](#)] [[PubMed](#)]
43. Bonanomi, D.; Pennuto, M.; Rigoni, M.; Rossetto, O.; Montecucco, C.; Valtorta, F. Taipoxin induces synaptic vesicle exocytosis and disrupts the interaction of synaptophysin I with VAMP2. *Mol. Pharmacol.* **2005**, *67*, 1901–1908. [[CrossRef](#)] [[PubMed](#)]
44. Lambeau, G.; Schmid-Alliana, A.; Lazdunski, M.; Barhanin, J. Identification and purification of a very high affinity binding protein for toxic phospholipases A₂ in skeletal muscle. *J. Biol. Chem.* **1990**, *265*, 9526–9532. [[CrossRef](#)]
45. Kolko, M.; Bruhn, T.; Christensen, T.; Lazdunski, M.; Lambeau, G.; Bazan, N.G.; Diemer, N.H. Secretory phospholipase A₂ potentiates glutamate-induced rat striatal neuronal cell death in vivo. *Neurosci. Lett.* **1999**, *274*, 167–170. [[CrossRef](#)]
46. Jabeen, T.; Sharma, S.; Singh, N.; Singh, R.K.; Kaur, P.; Perbandt, M.; Betzel, C.; Srinivasan, A.; Singh, T.P. Crystal structure of a calcium-induced dimer of two isoforms of cobra phospholipase A₂ at 1.6 Å resolution. *Proteins* **2005**, *59*, 856–863. [[CrossRef](#)]
47. Takasaki, C.; Kimura, S.; Kokubun, Y.; Tamiya, N. Isolation, properties and amino acid sequences of a phospholipase A₂ and its homologue without activity from the venom of a sea snake, *Laticauda colubrina*, from the Solomon Islands. *Biochem. J.* **1988**, *253*, 869–875. [[CrossRef](#)] [[PubMed](#)]
48. Halpert, J.; Eaker, D.; Karlsson, E. The role of phospholipase activity in the action of a presynaptic neurotoxin from the venom of *Notechis scutatus scutatus* (Australian tiger snake). *FEBS Lett.* **1976**, *61*, 72–76. [[CrossRef](#)]
49. Zimmerman, S.E.; Yong, L.C. Nephrotoxicity of notexin in experimental mice. *Exp. Toxicol. Pathol.* **1995**, *47*, 149–155. [[CrossRef](#)]
50. Kini, R.M.; Doley, R. Structure, function and evolution of three-finger toxins: Mini proteins with multiple targets. *Toxicon* **2010**, *56*, 855–867. [[CrossRef](#)]

51. Hiremath, K.; Dodakallanavar, J.; Sampat, G.H.; Patil, V.S.; Harish, D.R.; Chavan, R.; Hegde, H.V.; Roy, S. Three finger toxins of elapids: Structure, function, clinical applications and its inhibitors. *Mol. Divers.* **2024**, *28*, 3409–3426. [[CrossRef](#)] [[PubMed](#)]
52. Zamudio, F.; Wolf, K.M.; Martin, B.M.; Possani, L.D.; Chiappinelli, V.A. Two novel alpha-neurotoxins isolated from the taipan snake, *Oxyuranus scutellatus*, exhibit reduced affinity for nicotinic acetylcholine receptors in brain and skeletal muscle. *Biochemistry* **1996**, *35*, 7910–7916. [[CrossRef](#)]
53. Huynh, T.M.; Silva, A.; Isbister, G.K.; Hodgson, W.C. Isolation and pharmacological characterization of α -elapitoxin-Oh3a, a long-chain post-synaptic neurotoxin from King Cobra (*Ophiophagus hannah*) venom. *Front. Pharmacol.* **2022**, *13*, 815069. [[CrossRef](#)]
54. Diochot, S.; Baron, A.; Salinas, M.; Douguet, D.; Scarzello, S.; Dabert-Gay, A.S.; Debayle, D.; Friend, V.; Alloui, A.; Lazdunski, M.; et al. Black mamba venom peptides target acid-sensing ion channels to abolish pain. *Nature* **2012**, *490*, 552–555. [[CrossRef](#)]
55. Trummal, K.; Tönismägi, K.; Paalme, V.; Järvekülg, L.; Siigur, J.; Siigur, E. Molecular diversity of snake venom nerve growth factors. *Toxicon* **2011**, *58*, 363–368. [[CrossRef](#)] [[PubMed](#)]
56. Kweon, H.J.; Suh, B.C. Acid-sensing ion channels (ASICs): Therapeutic targets for neurological diseases and their regulation. *BMB Rep.* **2013**, *46*, 295–304. [[CrossRef](#)]
57. Storozhuk, M.; Cherninskyi, A.; Maximuk, O.; Isaev, D.; Krishtal, O. Acid-sensing ion channels: Focus on physiological and some pathological roles in the brain. *Curr. Neuropharmacol.* **2021**, *19*, 1570–1589.
58. Levi-Montalcini, R.; Angeletti, P.U. Essential role of the nerve growth factor in the survival and maintenance of dissociated sensory and sympathetic embryonic nerve cells in vitro. *Dev. Biol.* **1963**, *7*, 653–659. [[CrossRef](#)]
59. Paalme, V.; Trummal, K.; Samel, M.; Tönismägi, K.; Järvekülg, L.; Vija, H.; Subbi, J.; Siigur, J.; Siigur, E. Nerve growth factor from *Vipera lebetina* venom. *Toxicon* **2009**, *54*, 329–336. [[CrossRef](#)]
60. Fry, B.G. From genome to “venome”: Molecular origin and evolution of the snake venom proteome inferred from phylogenetic analysis of toxin sequences and related body proteins. *Genome Res.* **2005**, *15*, 403–420. [[CrossRef](#)] [[PubMed](#)]
61. Sunagar, K.; Fry, B.G.; Jackson, T.N.W.; Casewell, N.R.; Undheim, E.A.B.; Vidal, N.; Ali, S.A.; King, G.F.; Vasudevan, K.; Vasconcelos, V.; et al. Molecular evolution of vertebrate neurotrophins: Co-option of the highly conserved nerve growth factor gene into the advanced snake venom arsenal. *PLoS ONE* **2013**, *8*, e81827. [[CrossRef](#)]
62. Rocco, M.L.; Soligo, M.; Manni, L.; Aloe, L. Nerve growth factor: Early studies and recent clinical trials. *Curr. Neuropharmacol.* **2018**, *16*, 1455–1465. [[CrossRef](#)]
63. Capsoni, S.; Cattaneo, A. On the molecular basis linking Nerve Growth Factor (NGF) to Alzheimer’s disease. *Cell. Mol. Neurobiol.* **2006**, *26*, 619–633. [[CrossRef](#)] [[PubMed](#)]
64. Rosing, J.; Tans, G. Structural and functional properties of snake venom prothrombin activators. *Toxicon* **1992**, *30*, 1515–1527. [[CrossRef](#)] [[PubMed](#)]
65. Rosing, J.; Tans, G. Snake venom prothrombin activators—The history. In *Toxins and Hemostasis*; Springer: Dordrecht, The Netherlands, 2010; pp. 485–499.
66. Kini, R.M. The intriguing world of prothrombin activators from snake venom. *Toxicon* **2005**, *45*, 1133–1145. [[CrossRef](#)]
67. St Pierre, L.; Masci, P.P.; Filippovich, I.; Sorokina, N.; Marsh, N.; Miller, D.J.; Lavin, M.F. Comparative analysis of prothrombin activators from the venom of Australian elapids. *Mol. Biol. Evol.* **2005**, *22*, 1853–1864. [[CrossRef](#)] [[PubMed](#)]
68. Tacon, C.L.; Munas, A.; Little, M. Case report: Rotational thromboelastometry in taipan envenomation. *Am. J. Trop. Med. Hyg.* **2021**, *106*, 746–749. [[CrossRef](#)]
69. Waheed, H.; Moin, S.F.; Choudhary, M.I. Snake venom: From deadly toxins to life-saving therapeutics. *Curr. Med. Chem.* **2017**, *24*, 1874–1891. [[CrossRef](#)]
70. Daniels, L.B.; Maisel, A.S. Natriuretic peptides. *J. Am. Coll. Cardiol.* **2007**, *50*, 2357–2368. [[CrossRef](#)]
71. Nakao, K.; Ogawa, Y.; Suga, S.I.; Imura, H. Molecular biology and biochemistry of the natriuretic peptide system. In *Molecular Reviews in Cardiovascular Medicine*; Springer: Dordrecht, The Netherlands, 1996; pp. 74–82.
72. Fry, B.G.; Vidal, N.; Norman, J.A.; Vonk, F.J.; Scheib, H.; Ramjan, S.F.R.; Kuruppu, S.; Fung, K.; Hedges, S.B.; Richardson, M.K.; et al. Early evolution of the venom system in lizards and snakes. *Nature* **2006**, *439*, 584–588. [[CrossRef](#)]
73. Vink, S.; Jin, A.H.; Poth, K.J.; Head, G.A.; Alewood, P.F. Natriuretic peptide drug leads from snake venom. *Toxicon* **2012**, *59*, 434–445. [[CrossRef](#)] [[PubMed](#)]
74. Zhang, Y.; Wu, J.; Yu, G.; Chen, Z.; Zhou, X.; Zhu, S.; Li, R.; Zhang, Y.; Lu, Q. A novel natriuretic peptide from the cobra venom. *Toxicon* **2011**, *57*, 134–140. [[CrossRef](#)]
75. Chen, H.H.; Burnett Jr, J.C. Clinical application of the natriuretic peptides in heart failure. *Eur. Heart J. Suppl.* **2006**, *8*, E18–E25. [[CrossRef](#)]
76. Ang, W.F.; Koh, C.Y.; Kini, R.M. From snake venoms to therapeutics: A focus on natriuretic peptides. *Pharmaceuticals* **2022**, *15*, 1153. [[CrossRef](#)]
77. Krätzschar, J.; Haendler, B.; Eberspaecher, U.; Roosterman, D.; Donner, P.; Schleuning, W.D. The human cysteine-rich secretory protein (CRISP) family. Primary structure and tissue distribution of CRISP-1, CRISP-2 and CRISP-3. *Eur. J. Biochem.* **1996**, *236*, 827–836. [[CrossRef](#)]

78. Cohen, D.J.; Maldera, J.A.; Weigel Muñoz, M.; Ernesto, J.I.; Vasen, G.; Cuasnicu, P.S. Cysteine-Rich Secretory Proteins (CRISP) and their role in mammalian fertilization. *Biol. Res.* **2011**, *44*, 135–138. [[CrossRef](#)]
79. Yamazaki, Y.; Hyodo, F.; Morita, T. Wide distribution of cysteine-rich secretory proteins in snake venoms: Isolation and cloning of novel snake venom cysteine-rich secretory proteins. *Arch. Biochem. Biophys.* **2003**, *412*, 133–141. [[CrossRef](#)] [[PubMed](#)]
80. Tadokoro, T.; Modahl, C.M.; Maenaka, K.; Aoki-Shioi, N. Cysteine-rich secretory proteins (CRISPs) from venomous snakes: An overview of the functional diversity in a large and underappreciated superfamily. *Toxins* **2020**, *12*, 175. [[CrossRef](#)] [[PubMed](#)]
81. Snutch, T.P. Voltage-Gated Calcium Channels. In *Encyclopedia of Neuroscience*; Elsevier: Amsterdam, The Netherlands, 2009; pp. 427–441.
82. Yamazaki, Y.; Brown, R.L.; Morita, T. Purification and cloning of toxins from elapid venoms that target cyclic nucleotide-gated ion channels. *Biochemistry* **2002**, *41*, 11331–11337. [[CrossRef](#)]
83. Lecht, S.; Chiaverelli, R.A.; Gerstenhaber, J.; Calvete, J.J.; Lazarovici, P.; Casewell, N.R.; Harrison, R.; Lelkes, P.I.; Marcinkiewicz, C. Anti-angiogenic activities of snake venom CRISP isolated from *Echis carinatus sochureki*. *Biochim. Biophys. Acta* **2015**, *1850*, 1169–1179. [[CrossRef](#)]
84. Adade, C.M.; Carvalho, A.L.O.; Tomaz, M.A.; Costa, T.F.R.; Godinho, J.L.; Melo, P.A.; Lima, A.P.C.A.; Rodrigues, J.C.F.; Zingali, R.B.; Souto-Pradón, T. Crovirin, a snake venom cysteine-rich secretory protein (CRISP) with promising activity against Trypanosomes and *Leishmania*. *PLoS Negl. Trop. Dis.* **2014**, *8*, e3252. [[CrossRef](#)]
85. Zupunski, V.; Kordis, D.; Gubensek, F. Adaptive evolution in the snake venom Kunitz/BPTI protein family. *FEBS Lett.* **2003**, *547*, 131–136. [[CrossRef](#)]
86. Ranasinghe, S.; McManus, D.P. Structure and function of invertebrate Kunitz serine protease inhibitors. *Dev. Comp. Immunol.* **2013**, *39*, 219–227. [[CrossRef](#)]
87. Kunitz, M.; Northrop, J.H. Isolation from beef pancreas of crystalline trypsinogen, trypsin, a trypsin inhibitor, and an inhibitor trypsin compound. *J. Gen. Physiol.* **1936**, *19*, 991–1007. [[CrossRef](#)]
88. Huber, R.; Kukla, D.; Rhlmann, A.; Epp, O.; Formanek, H. The basic trypsin inhibitor of bovine pancreas. *Sci. Nat.* **1970**, *57*, 389–392. [[CrossRef](#)]
89. Millers, E.K.I.; Trabi, M.; Masci, P.P.; Lavin, M.F.; de Jersey, J.; Guddat, L.W. Crystal structure of textilinin-1, a Kunitz-type serine protease inhibitor from the venom of the Australian common brown snake (*Pseudonaja textilis*). *FEBS J.* **2009**, *276*, 3163–3175. [[CrossRef](#)] [[PubMed](#)]
90. Chen, C.; Hsu, C.H.; Su, N.Y.; Lin, Y.C.; Chiou, S.H.; Wu, S.H. Solution structure of a Kunitz-type chymotrypsin inhibitor isolated from the elapid snake *Bungarus fasciatus*. *J. Biol. Chem.* **2001**, *276*, 45079–45087. [[CrossRef](#)] [[PubMed](#)]
91. Harvey, A.L. Twenty years of dendrotoxins. *Toxicon* **2001**, *39*, 15–26. [[CrossRef](#)]
92. Schweitz, H.; Heurteaux, C.; Bois, P.; Moinier, D.; Romey, G.; Lazdunski, M. Calciudine, a venom peptide of the Kunitz-type protease inhibitor family, is a potent blocker of high-threshold Ca²⁺ channels with a high affinity for L-type channels in cerebellar granule neurons. *Proc. Natl. Acad. Sci. USA* **1994**, *91*, 878–882. [[CrossRef](#)] [[PubMed](#)]
93. Droctové, L.; Ciolek, J.; Mendre, C.; Chorfa, A.; Huerta, P.; Carvalho, C.; Gouin, C.; Lancien, M.; Stanajic-Petrovic, G.; Braco, L.; et al. A new Kunitz-type snake toxin family associated with an original mode of interaction with the vasopressin 2 receptor. *Br. J. Pharmacol.* **2022**, *179*, 3470–3481. [[CrossRef](#)]
94. Morjen, M.; Honoré, S.; Bazaa, A.; Abdelkafi-Koubaa, Z.; Ellafi, A.; Mabrouk, K.; Kovacic, H.; El Ayeb, M.; Marrakchi, N.; Luis, J. PIVL, a snake venom Kunitz-type serine protease inhibitor, inhibits in vitro and in vivo angiogenesis. *Microvasc. Res.* **2014**, *95*, 149–156. [[CrossRef](#)]
95. Morjen, M.; Kallech-Ziri, O.; Bazaa, A.; Othman, H.; Mabrouk, K.; Zouari-Kessentini, R.; Sanz, L.; Calvete, J.J.; Srairi-Abid, N.; El Ayeb, M.; et al. PIVL, a new serine protease inhibitor from *Macrovipera lebetina transmediterranea* venom, impairs motility of human glioblastoma cells. *Matrix Biol.* **2013**, *32*, 52–62. [[CrossRef](#)]
96. Mukherjee, A.K.; Mackessy, S.P. Pharmacological properties and pathophysiological significance of a Kunitz-type protease inhibitor (Rusvikunin-II) and its protein complex (Rusvikunin complex) purified from *Daboia russelii russelii* venom. *Toxicon* **2014**, *89*, 55–66. [[CrossRef](#)]
97. Jeong, J.K.; Diano, S. Prolyl carboxypeptidase and its inhibitors in metabolism. *Trends Endocrinol. Metab.* **2013**, *24*, 61–67. [[CrossRef](#)] [[PubMed](#)]
98. Graham, T.H. Prolylcarboxypeptidase (PrCP) inhibitors and the therapeutic uses thereof: A patent review. *Expert. Opin. Ther. Pat.* **2017**, *27*, 1077–1088. [[CrossRef](#)] [[PubMed](#)]
99. Beraldo-Neto, E.; Vigerelli, H.; Coelho, G.R.; da Silva, D.L.; Nencioni, A.L.A.; Pimenta, D.C. Unraveling and profiling *Tityus bahiensis* venom: Biochemical analyses of the major toxins. *J. Proteom.* **2023**, *274*, 104824. [[CrossRef](#)] [[PubMed](#)]

Disclaimer/Publisher’s Note: The statements, opinions and data contained in all publications are solely those of the individual author(s) and contributor(s) and not of MDPI and/or the editor(s). MDPI and/or the editor(s) disclaim responsibility for any injury to people or property resulting from any ideas, methods, instructions or products referred to in the content.